

## Real-time model predictive control of structures under earthquakes

Gang Mei<sup>1</sup>, Ahsan Kareem<sup>2,\*</sup>,† and Jeffrey C. Kantor<sup>3</sup>

<sup>1</sup>*NatHaz Modeling Laboratory, Department of Civil Engineering and Geological Sciences,  
University of Notre Dame, Notre Dame, IN 46556, U.S.A.*

<sup>2</sup>*Department of Civil Engineering and Geological Sciences, University of Notre Dame, Notre Dame,  
IN 46556, U.S.A.*

<sup>3</sup>*Department of Chemical Engineering, University of Notre Dame, Notre Dame, IN 46556, U.S.A.*

### SUMMARY

This paper presents a general formulation of the model predictive control (MPC) scheme for controlling in real time the response of structures under earthquakes. The MPC scheme is based on an explicit use of a prediction model of the system response to obtain the control actions by minimizing an objective function. Optimization objectives in MPC include minimization of the difference between the predicted and desired response trajectories, and the control effort subjected to certain constraints. In this study, the prediction model is formulated using both feedforward (FF) and feedback (FB) components to increase the effectiveness of the MPC scheme. The FF loop in the prediction model is formulated using two types of input. First, it is designed using the established Kanai–Tajimi-type model to represent the earthquake input. Second, a real-time FF loop is introduced using an auto-regressive (AR) model for earthquake ground motion which is constantly updated using real-time on-line observations. The real-time FF loop certainly promises to add predictive and adaptive features to the control actions to account for any unusual features in the ground motion. The structural response with and without the FF and FB loops are compared. Examples are used to demonstrate the efficacy of the proposed methodology. These examples show that the MPC-based controller is effective in reducing the structural response under different earthquakes which contain distinct features in their spectral and non-stationary descriptions. The performance of the MPC scheme is then compared to  $H_2$  control strategies for different time horizons. The effectiveness of MPC is shown to be equivalent to the optimal control. This paper lays a foundation for capturing the main strengths of MPC, i.e. computational expediency, real-time application, intrinsic compensation for time delays, treatment of constraints and potential for future extensions in structural control. Copyright © 2001 John Wiley & Sons, Ltd.

KEY WORDS: model predictive control; real time

---

\* Correspondence to: Ahsan Kareem, Department of Civil Engineering and Geological Sciences, University of Notre Dame, 156 Fitzpatrick Hall, Notre Dame, Indiana 46556-5602, U.S.A.

Contract/grant sponsor: National Science Foundation; contract/grant number: CMS-94-02196

Contract/grant sponsor: NSF Structure Control Initiative; contract/sponsor number: CMS-95-03779

## 1. INTRODUCTION

Structural control is an attractive option for improving the performance of a variety of structures, including bridges, tall buildings, and offshore structures. The performance of such systems under environmental loads has improved greatly as a result of theoretical and experimental research and related development efforts [1–9]. A comprehensive review of theoretical developments in control design can be found in Reference [10]. Details concerning their applications to real structures can be found in Reference [11]. Benchmark problems conducted to assess the performance of different control strategies can be found in Reference [4]. The most commonly used scheme in controller design is linear quadratic regulator (LQR). Other schemes like the  $H_2$  and  $H_\infty$  were introduced in civil engineering and applied to structural control design [2, 12–15]. The sliding mode control has been introduced by Utkin [16] and its potential applications have been given by Slotine [17] and Yang *et al.* [3]. Other schemes include the predictive control which has been used in structural applications [18]. Lopez-Almansa *et al.* [19] employed a modal approach in which the first few modes were controlled to reduce the overall structural response. In a companion paper they presented this modal approach experimentally [20].

Most of the control strategies reported in the literature have been based only on the FB control. However, some studies also utilized a FF compensator which works in conjunction with a FB loop (e.g., References [2, 13, 15, 21–23]). In this FF–FB scheme, the equations of structural motion are augmented with an appropriate state-space excitation model that is based on a filtered Gaussian white noise process. The FF loops can be formulated using two types of input. First, the FF loops can be based on established spectral characteristics of the excitation (e.g. earthquakes, wind, and waves). Second, the FF loops can be based on actual measurements and on-line models fitted to the data (e.g. the auto-regressive (AR) model). These loops are then used in conjunction with the equations of motion to determine both FF and FB gains. Suhardjo *et al.* [2, 13] and Suhardjo and Kareem [5] presented the frequency-domain optimal control of earthquake, wind and wave excited structures using FF–FB control schemes. Yamada and Kobori [21] used an AR model to fit on-line measurements of ground acceleration into a state-space excitation model and used the LQR control to obtain the FF–FB gains. Their results demonstrated that the FF–FB strategy enhanced the performance of the controller.

MPC has been effectively used in chemical, automotive and aerospace industries [24–27]. MPC has been shown to be feasible for structural control applications by Mei *et al.* [22]. The underlying concept of MPC is that the future behaviour of a structure is predicted from its present response using a system dynamics model and control actions are determined so as to optimize future structural behaviour over a prediction horizon. MPC offers a general framework of posing the control problem in the time domain and can be used to integrate issues of the optimal control, stochastic control, control of processes, with time delays, multivariable control and future references. The concept is not limited to a particular system description, but the computation and implementation depend on the model representation, e.g. state space, transfer matrix, etc., Inclusion of constraints is conceptually simple and can be systematically included during the design and implementation of the controller.

In this study, MPC is employed in conjunction with the FF–FB strategy to reduce structural response under earthquake excitation. First, the Kanai–Tajimi earthquake model is used to model the FF component of the FF–FB control. Next, a formulation of MPC with an AR

model embedded in the FF loop is presented. In this manner, a real-time FF link is included to introduce predictive and adaptive features to account for seismic events with unusual dynamic features. The AR model in the FF loop is based on initial observations of the ground motion. The model is constantly updated using new information. The time-series-based model is then used to represent the state equations of the excitation. Finally, the structural system equations are augmented with the excitation model to include real-time earthquake input.

A single- and a three-storey building examples are used to demonstrate the methodology. The MPC-AR controller is shown to be effective in reducing structural response under a host of earthquakes that contain distinct spectral and transient features. The results of the MPC analysis are also compared with the  $H_2$ -based control schemes.

The effectiveness of MPC is demonstrated to be equivalent to the optimal control. This paper lays a foundation for capturing the main strengths of MPC, i.e. computational expediency, real-time applications, intrinsic compensation for time delays, treatment of constraints and potential for future extensions in structural control.

## 2. PROBLEM FORMULATION

A building exposed to seismic excitation is modelled as an  $n$ -degree-of-freedom system:

$$\mathbf{M}\ddot{x} + \mathbf{C}\dot{x} + \mathbf{K}x = \mathbf{F} - \mathbf{M}\mathbf{I}\ddot{x}_g \tag{1}$$

where  $\mathbf{M}$ ,  $\mathbf{C}$ , and  $\mathbf{K}$  are the mass, damping and stiffness matrices, respectively;  $x$ ,  $\dot{x}$  and  $\ddot{x}$  are the  $n \times 1$  displacement, velocity and acceleration vectors relative to the ground;  $\mathbf{I}$  is the  $n \times 1$  identity vector;  $\ddot{x}_g$  is the ground acceleration and  $\mathbf{F} = \mathbf{L}u$  is the  $n \times 1$  control force vector generated by placing the actuator on different floors.  $\mathbf{L}$  is an  $n \times m$  matrix with elements equal to zero or one depending on the placement of the actuator on different floors and  $u$  is an  $m \times 1$  control force vector. Equation (1) is expressed in a state-space format as follows:

$$\begin{aligned} \dot{\mathbf{x}} = \begin{bmatrix} \dot{x} \\ \ddot{x} \end{bmatrix} &= \begin{bmatrix} 0 & \mathbf{I} \\ -\mathbf{M}^{-1}\mathbf{K} & -\mathbf{M}^{-1}\mathbf{C} \end{bmatrix} \begin{bmatrix} x \\ \dot{x} \end{bmatrix} + \begin{bmatrix} 0 \\ \mathbf{M}^{-1}\mathbf{L} \end{bmatrix} u + \begin{bmatrix} 0 \\ \mathbf{I} \end{bmatrix} \ddot{x}_g \\ &= \mathbf{A}\mathbf{x} + \mathbf{B}u + \mathbf{G}\ddot{x}_g \end{aligned} \tag{2}$$

where  $\mathbf{G}$  is a vector that represents the seismic load distribution.

For digital implementation of control, Equation (2) is expressed in discrete time as

$$\mathbf{x}((k + 1)T) = \Phi\mathbf{x}(kT) + \Gamma_u u(kT) + \Gamma_d \ddot{x}_g(kT) \tag{3}$$

where  $\Phi = e^{\mathbf{A}T}$  is a  $2n \times 2n$  matrix,  $\Gamma_u = \mathbf{P}_1\mathbf{B}$  and  $\Gamma_d = \mathbf{P}_1\mathbf{G}$  are  $2n \times m$  matrices for which  $\mathbf{P}_1 = \int_0^T e^{\mathbf{A}\tau} d\tau$  is a  $2n \times 2n$  matrix and  $T$  is the sampling time.

### 3. FEEDFORWARD MODEL

#### 3.1. Pre-established earthquake model: Kanai–Tajimi

The earthquake signal can be modelled as filtered white noise process, the filter design is based on a prescribed spectrum of ground motion, e.g. the Kanai–Tajimi model [28]. In this discussion, the Kanai–Tajimi spectral description of the ground motion is used:

$$S(\omega) = S_0 \left[ \frac{\omega_g^4 + 4\omega_g^2 \zeta_g^2 \omega^2}{(\omega^2 - \omega_g^2)^2 + 4\omega_g^2 \zeta_g^2 \omega^2} \right] \quad (4)$$

where  $\zeta_g$ ,  $\omega_g$  and  $S_0$  are parameters which depend on the site soil characteristics and seismic intensity. The transient or non-stationary feature of the earthquake is introduced through an amplitude modulating function [29].

The transfer function is then decomposed to get the state-space realization of the earthquake signal. The state-space representation can be expressed as

$$\begin{aligned} r(k+1) &= A_r r(k) + B_r e_r(k) \\ d(k) &= C_r(k) r(k) \end{aligned} \quad (5)$$

where  $r(k)$  is a two-dimensional vector containing the states of the seismic excitation model,  $e_r(k)$  is a stationary Gaussian vector white noise process and  $C_r(k)$  is a time-varying vector that includes non-stationary excitation in this model. The matrices in the excitation model are given by

$$A_r = \begin{bmatrix} 0 & 1 \\ -\omega_g^2 & -2\zeta_g \omega_g \end{bmatrix}, \quad B_r = \begin{bmatrix} 0 \\ 1 \end{bmatrix}, \quad C_r(k) = g(k) [-\omega_g^2 \quad -2\zeta_g \omega_g] \quad (6)$$

where  $g(k)$  is a modulating function chosen to reflect the transient nature of the time-dependent ground acceleration. This dynamic earthquake model can then be combined with the state-space model of the structure to get an augmented state-space equation, which is used to perform FF–FB control.

#### 3.2. Real-time model of earthquake

The ground acceleration time history can be introduced using a time-varying auto-regressive (AR) model to reflect the non-stationary features of ground motion. At each time instant  $t_k = kT$ , a  $p$ -dimensional AR model is formulated using the Yule–Walker equation. The simulated seismic excitation at time  $t_k$  is defined as  $d(k)$ . The error,  $e_r(k)$ , between the measured and the modelled excitation is then obtained at each step. The AR model is expressed in the state-space form and is subsequently embedded in the overall system state-space equations as follows:

$$\begin{aligned} r(k+1) &= A_r(k) r(k) + B_r(k) e_r(k) \\ d(k) &= C_r(k) r(k) + D_r(k) e_r(k) \end{aligned} \quad (7)$$

where

$$r(k) = [d^T(k-p) \quad d^T(k-p+1) \quad \dots \quad d^T(k-2) \quad d^T(k-1)]^T \tag{8}$$

$$A_r(k) = \begin{bmatrix} 0 & 1 & \dots & 0 \\ \dots & \dots & \dots & \dots \\ 0 & 0 & \dots & 1 \\ -a_p(k) & \dots & \dots & -a_1(k) \end{bmatrix}, \quad B_r(k) = [0 \quad \dots \quad 1]$$

$$C_r(k) = -b_0(k)[a_p(k) \quad \dots \quad a_1(k)], \quad D_r(k) = b_0(k) \tag{9}$$

$a_p(k), a_{p-1}(k), \dots, a_1(k), b_0(k)$  are obtained from the AR model at time  $t_k$ .

#### 4. STRUCTURE-EXCITATION MODEL

The building model described in Section 2 and the earthquake model given in Section 3 or Section 4 are then combined to establish an augmented overall system model. From Equations (3) and (7), the following augmented state-space representation is obtained:

$$z(k+1) = \hat{\Phi}(k)z(k) + \hat{\Gamma}_u(k)u(k) + \hat{\Gamma}_d(k)e_r(k) \tag{10}$$

in which

$$\begin{aligned} z(k+1) &= \begin{bmatrix} x(k+1) \\ r(k+1) \end{bmatrix}, \quad \hat{\Phi}(k) = \begin{bmatrix} \Phi & \Gamma_d C_r(k) \\ 0 & A_r(k) \end{bmatrix}, \\ \hat{\Gamma}_u(k) &= \begin{bmatrix} \Gamma_u \\ 0 \end{bmatrix}, \quad \hat{\Gamma}_d(k) = \begin{bmatrix} \Gamma_d D_r(k) \\ B_r(k) \end{bmatrix} \end{aligned} \tag{11}$$

For the Kanai–Tajimi model  $D_r(k) = 0$ .

#### 5. MODEL PREDICTIVE CONTROL (MPC) SCHEME

The MPC scheme is based on an explicit use of a prediction model of the system response to obtain the control action by minimizing an objective function. Optimization objectives include minimization of the difference between the predicted and reference response and the control effort subject to certain constraints such as limits on the magnitude of the control force. This concept is illustrated in Figure 1(a). First a reference trajectory,  $y_r(k)$ , is specified. The reference trajectory is the desired target trajectory for the process output. This is followed by an appropriate prediction model which is then used to determine the future building responses,  $\hat{y}(k)$ . The prediction model must be able to include the dynamic processes while remaining simple enough to implement and understand. The prediction is made over a pre-established extended time horizon using the current time as the prediction origin. For a discrete-time model, this means predicting  $\hat{y}(k+1), \hat{y}(k+2), \dots, \hat{y}(k+i)$  for  $i$  sample times in the future.

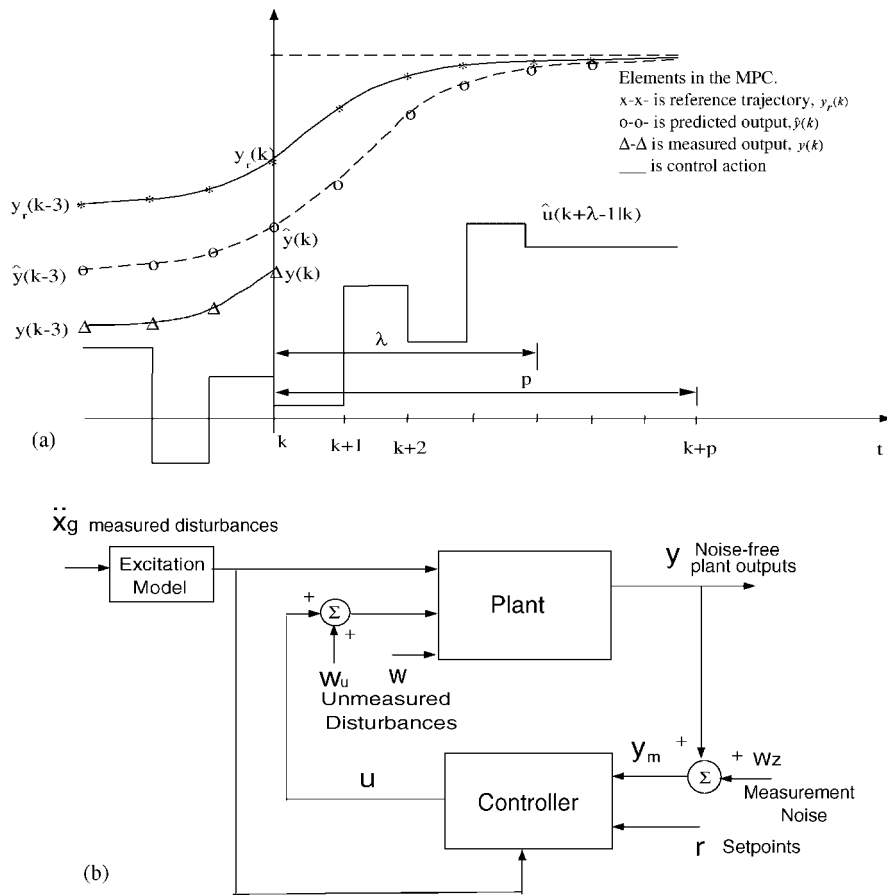


Figure 1. (a) Basic MPC scheme. (b) FF-FB control system.

This prediction is based on both actual past control inputs  $u(k), u(k-1), \dots, u(k-j)$  and on the sequence of future control efforts determined using the prediction model that are needed to satisfy a prescribed optimization objective. The control signals that are determined using the prediction model are then applied to the structure, and the actual system output,  $y(k)$ , is found. Finally, the actual measurement,  $y(k)$ , is compared to the model prediction  $\hat{y}(k)$  and the prediction error ( $\hat{e}(k) = y(k) - \hat{y}(k)$ ) is utilized to update future predictions. The plant input can be of various types as shown in Figure 1(b).

In the general model predictive control, the discrete-time state-space equations of the system are expressed as

$$\begin{aligned} \mathbf{x}(k+1) &= \Phi \mathbf{x}(k) + \Gamma U(k) \\ \mathbf{y}(k) &= C \mathbf{x}(k) + D U(k) \end{aligned} \tag{12}$$

where  $U(k) = [u^T(k) \ \ddot{x}_g^T(k) \ w_u^T(k) \ w^T(k) \ w_z^T(k)]^T$ ;  $w_u(k)$ ,  $w(k)$  and  $w_z(k)$  could be combined into a single unmeasured disturbance variable entering at the plant output. The unmeasured disturbance terms,  $w_u(k)$ ,  $w_k$  and  $w_z(k)$  are set equal to zero.

When a structure-excitation model with an embedded AR model is used the overall system states are increased. The prediction model is then expressed as

$$\hat{z}(k + 1|k) = \hat{\Phi}\hat{z}(k|k - 1) + \hat{\Gamma}_u\hat{u}(k|k - 1) + \hat{\Gamma}_d e_r(k|k) + \hat{\Gamma}_e \hat{e}(k|k) \tag{13}$$

$$\hat{y}(k|k - 1) = C\hat{z}(k|k - 1) \tag{14}$$

where  $\hat{z}(k + 1|k)$  estimates the state at a future sampling period,  $k + 1$ , using the information available at time step  $k$ ,  $\hat{y}(k|k - 1)$  estimates the structural output at time  $k$  based on information at  $k - 1$ ,  $C = [I \ 0]$ ,  $\hat{\Gamma}_e$  is a constant estimator gain matrix; and  $\hat{e}(k|k)$  is the estimated error defined as  $\hat{e}(k|k) = y(k) - \hat{y}(k|k - 1)$ .

Using Equation (10), the process output predicted at the  $k$ th step and the subsequent time steps  $k + j$ ,  $j = 1, \dots, p$  can be expressed as a function of the current state vector  $z(k)$  and the control vector  $u(k)$  as follows:

$$\Psi(k) = H\mathbf{u}(k) + Y_z\hat{z}(k|k - 1) + Y_d e_r(k) + Y_e \hat{e}(k|k) \tag{15}$$

$$\Psi(k) = [\hat{y}^T(k + 1|k) \dots \hat{y}^T(k + p|k)]^T, \quad \mathbf{u}(k) = [\hat{u}(k + 1|k) \dots \hat{u}(k + \lambda - 1|k)]^T \tag{16}$$

The reference output can be written as  $\Psi_r(k) = [y_r^T(k + 1|k) \dots y_r^T(k + p|k)]^T$  where  $p$  is the prediction horizon and  $\lambda$  is the control horizon.

The control objective function is given by

$$J = \frac{1}{2}[\Psi(k) - \Psi_r(k)]^T \bar{Q}[\Psi(k) - \Psi_r(k)] + \frac{1}{2}\mathbf{u}^T(k) \bar{R}\mathbf{u}(k) \tag{17}$$

By minimizing  $J$ , the optimal predictive control force is given by

$$\mathbf{u} = [H^T \bar{Q}H + \bar{R}]^{-1} H^T \bar{Q}[Y_z\hat{z}(k|k - 1) + Y_d e_r(k) + Y_e \hat{e}(k|k)] \tag{18}$$

in which  $H$ ,  $\bar{Q}$ ,  $\bar{R}$ ,  $Y_z$ ,  $Y_d$  and  $Y_e$  are given in the appendix.

The MPC formulation presented in the preceding section is utilized in the following examples to demonstrate its application to building structures.

## 6. NUMERICAL EXAMPLES AND ANALYSIS

The equation of motion for the single-degree-of-freedom system shown with cable bracing in Figure 2 is given by

$$\ddot{x}_0(t) + 2\zeta\omega_0\dot{x}_0(t) + \omega_0^2x_0(t) = -\ddot{x}_g(t) - \frac{4k_c \cos \alpha}{m}u_0(t) \tag{19}$$

where  $x_0$ ,  $\dot{x}_0$ , and  $\ddot{x}_0$  are the horizontal relative displacement, velocity and acceleration of the first floor;  $\ddot{x}_g$  is the ground acceleration;  $u_0$  is the actuator displacement;  $m$ ,  $\zeta$  and  $\omega_0$  are the

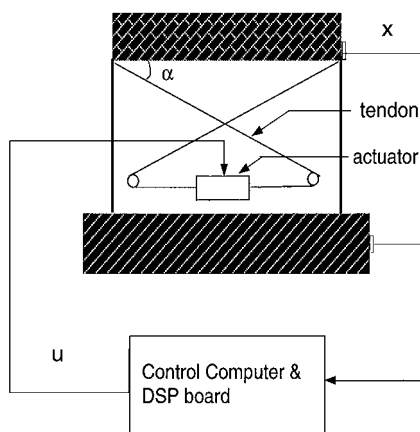


Figure 2. SDOF active tendon system.

mass, damping and angular frequency, respectively;  $k_c$  is the stiffness of the cable and  $\alpha$  is the cable angle. These parameters are defined as  $m = 2922.7$  kg,  $\zeta = 0.0124$ ,  $\omega_0 = 21.79$  rad/s,  $k_c = 371950.8$  N/m, and  $\alpha = 36^\circ$ .

The earthquake input to the building can be formulated in two ways. One approach involves modelling earthquake using the Kanai–Tajimi spectral model. The other utilizes the actual measurements to model the real-time excitation using an AR model. Details of both are discussed in the following section. The actual system response is then used to estimate the control force defined by the MPC strategy. An actuator may be used to introduce tension in cables to meet the desired response control objective. The dynamic control–structure interaction is not considered here in this study. However, as shown in Reference [30], it can be accounted for by including the dynamics of the actuator in the overall system model.

### 6.1. Kanai–Tajimi spectral model

In this example, first the earthquake excitation is generated using the Kanai–Tajimi spectral model. Details are given in Section 3. The prediction and control horizons are chosen to be 5 and 2, respectively. The weighting matrices are  $Q = I_{(2 \times 2)}$  and  $R = 100$ .

Figure 3 compares the displacement responses without control (dash line) and with MPC control using the Kanai–Tajimi model (solid line). Figures 4, 5 and 6 compare the displacement, acceleration response, and control force using MPC control alone (dash line) and MPC control using the Kanai–Tajimi model (solid line). It is noted that the FF–FB case (MPC plus Kanai–Tajimi) performs better than the FB case (MPC alone) as shown in figures. Table I lists numerical values obtained by utilizing the MPC FB and MPC FF–FB schemes. Clearly, the FF–FB control of MPC is better than the FB control alone. Using almost the same control force, the MPC FF–FB control produces a higher response reduction than the MPC FB control.

The prescribed spectral model can be implemented either off- or on-line, which requires that the spectral density of the earthquake excitation be known *a priori*. This is not practical, and may only be effective in cases when the earthquake characteristics match the prescribed spectral model, e.g. the Kanai–Tajimi model. The effectiveness of the control action could

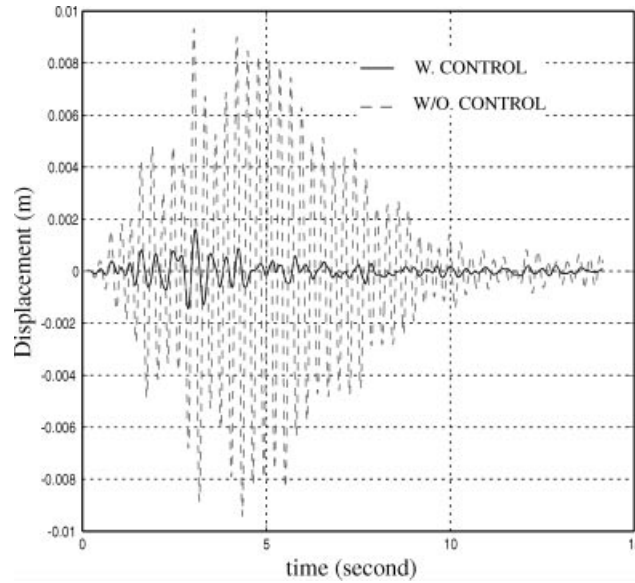


Figure 3. Displacement response without control and with MPC/Kanai-Tajimi scheme, ( $\lambda = 2, p = 5, R = 100$ ).

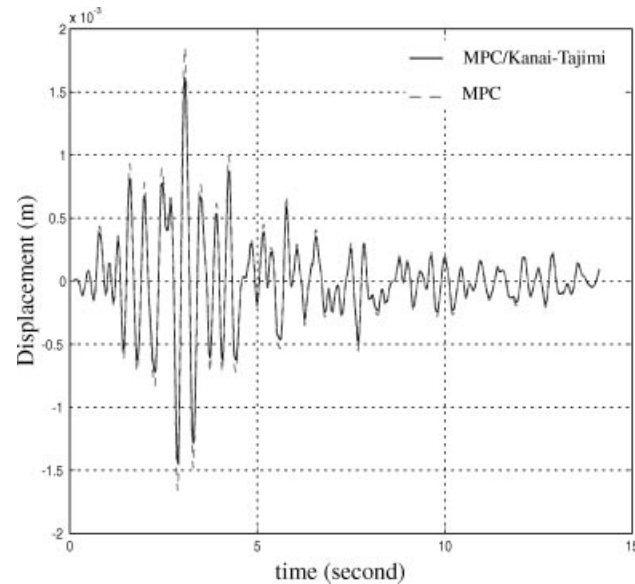


Figure 4. Displacement response using MPC/Kanai-Tajimi and MPC schemes ( $\lambda = 2, p = 5, R = 100$ ).

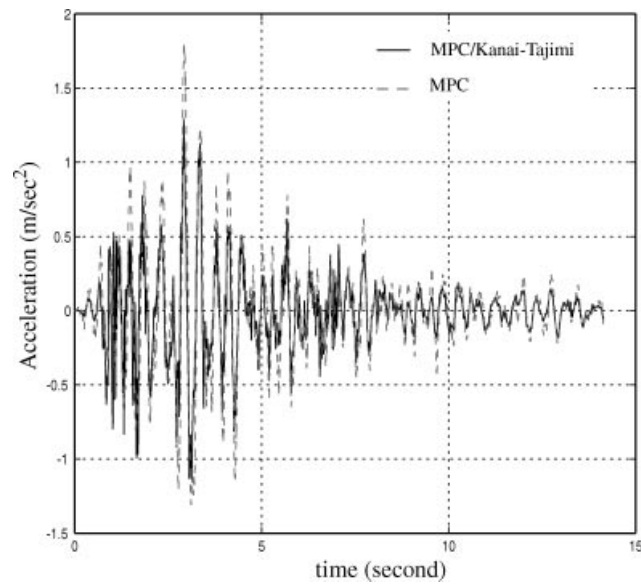


Figure 5. Acceleration using MPC/Kanai-Tajimi model and MPC schemes ( $\lambda = 2$ ,  $p = 5$ ,  $R = 100$ ).

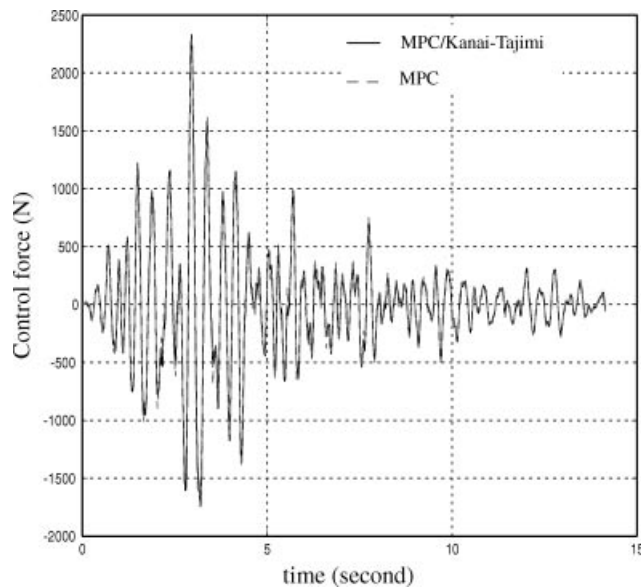


Figure 6. Control forces using MPC/Kanai-Tajimi model and MPC schemes ( $\lambda = 2$ ,  $p = 5$ ,  $R = 100$ ).

Table I. Comparison between the MPC/Kanai–Tajimi model and MPC.

	$\sigma_x$ (cm)	$\sigma_{\ddot{x}}$ (cm/s <sup>2</sup> )	$\sigma_u$ (kN)	$x_{\max}$ (cm)	$\ddot{x}_{\max}$ (cm/s <sup>2</sup> )	$u_{\max}$ (kN)
Without control	0.31	141.5	—	0.94	447.7	—
MPC	$3.77 \times 10^{-2}$	35.4	0.453	0.19	181.1	2.297
Percentage change	88%	75%	—	80%	60%	—
MPC/Kanai–Tajimi	$3.28 \times 10^{-2}$	25.8	0.455	0.16	129.3	2.334
Percentage change	90%	82%	0.38%	93%	71%	1.6%

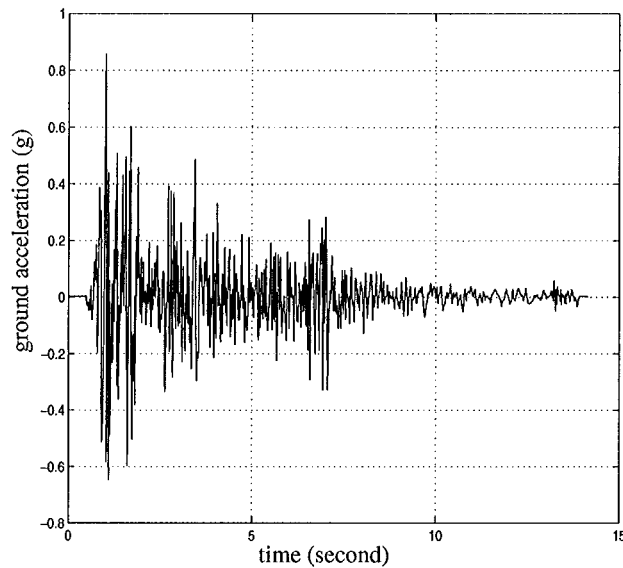


Figure 7. 1940 El Centro earthquake.

be reduced if the earthquake characteristics are either different from the Kanai–Tajimi model or change rapidly. In order to overcome this shortcoming, in the following case, a real-time model based on actual measurements is utilized.

### 6.2. MPC-AR control scheme

The FF based on AR modelling provides a practical way to apply the FF–FB control scheme more effectively. The 1940 El Centro earthquake record (Figure 7) was scaled to 0.25 of its maximum intensity and used in this analysis to excite the example building. Figures 8 and 9 compare the displacement and acceleration obtained using no control (dash line) with those obtained using the MPC-AR model (solid line). Both the displacement and acceleration responses are significantly reduced in the presence of the controller. Figures 10 and 11 compare the displacement and acceleration response obtained using the MPC alone (dash line) with those obtained using MPC-AR (solid line). The corresponding control forces are given in Figure 12. Table II lists comparisons of the response using no control, MPC alone, and

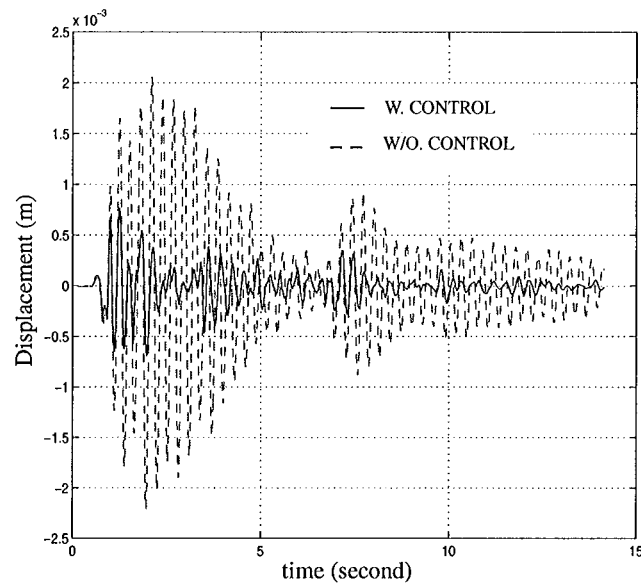


Figure 8. Comparison of uncontrolled building displacement with MPC-AR scheme ( $\lambda = 2$ ,  $p = 5$ ,  $R = 500$ ).

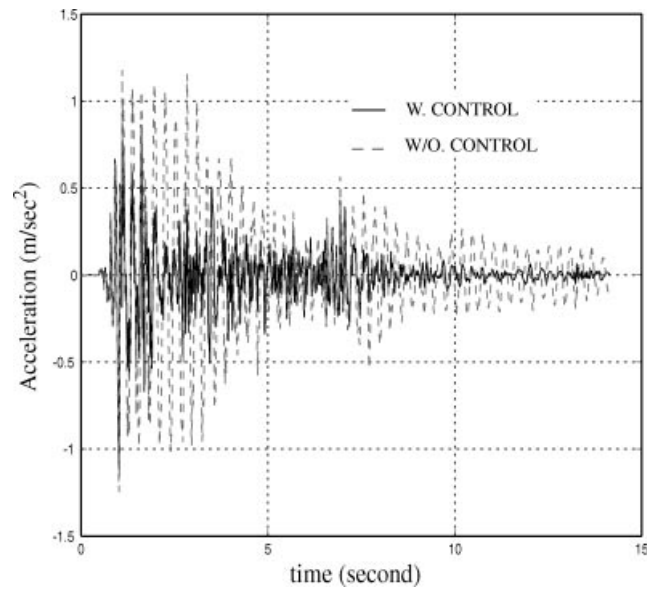


Figure 9. Comparison of uncontrolled building acceleration with MPC-AR scheme ( $\lambda = 2$ ,  $p = 5$ ,  $R = 500$ ).

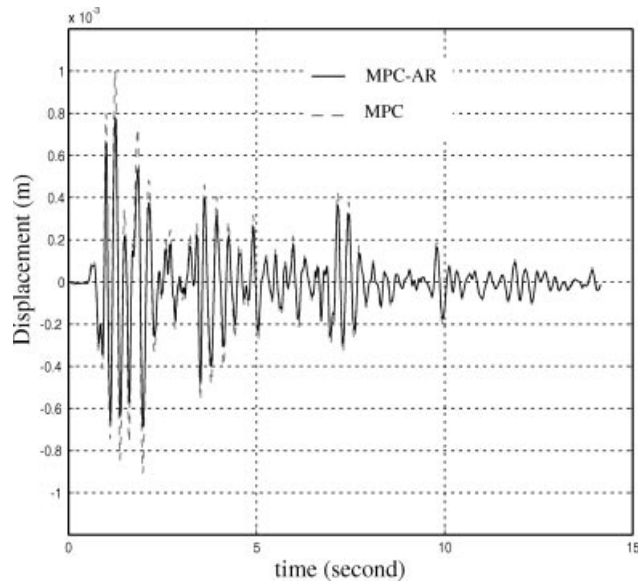


Figure 10. Comparison of displacement response.

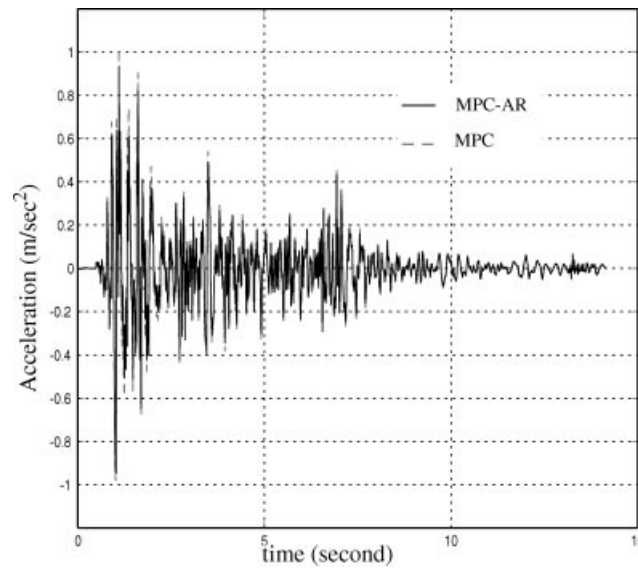


Figure 11. Comparison of acceleration response between MPC-AR and MPC schemes ( $\lambda = 2, p = 5, R = 500$ ).

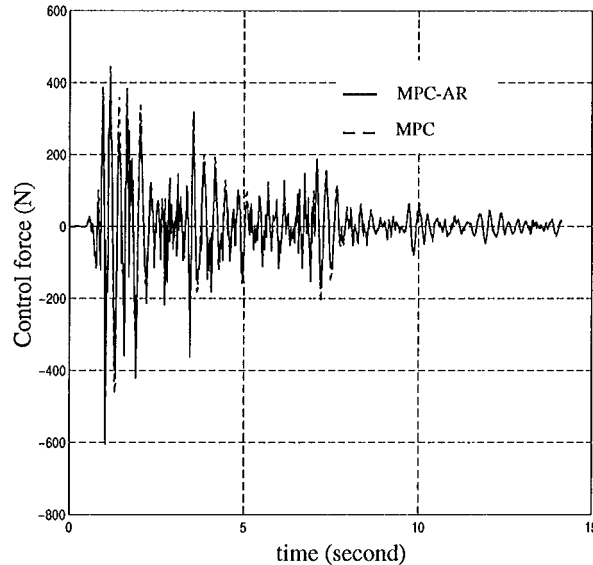


Figure 12. Comparison of control forces between MPC-AR and MPC schemes ( $\lambda = 2$ ,  $p = 5$ ,  $R = 500$ ).

Table II. Comparison between the MPC-AR model and MPC.

	$\sigma_x$ (cm)	$\sigma_{\ddot{x}}$ (cm/s <sup>2</sup> )	$\sigma_u$ (kN)	$x_{\max}$ (cm)	$\ddot{x}_{\max}$ (cm/s <sup>2</sup> )	$u_{\max}$ (kN)
Without control	$7.53 \times 10^{-2}$	37.8	—	0.25	135.4	—
MPC	$2.01 \times 10^{-2}$	14.6	0.099	0.10	101.5	0.672
Percentage change	73.3%	61.3%	—	60.0%	25.0%	—
MPC-AR	$1.60 \times 10^{-2}$	13.4	0.083	$7.80 \times 10^{-2}$	95.1	0.622
Percentage change	78.3%	64.4%	-15.6%	68.8%	29.7%	-7.37%

MPC-AR. The results show that when the MPC-AR model is used, the control performance is better than the scheme using MPC alone and furthermore, the control force is smaller. Clearly, the FF-FB control is more effective than the FB control scheme.

The performance of MPC scheme is compared to the  $H_2$  control strategies. In Figure 13, the root mean square (rms) value of the displacement and control force obtained using the MPC and  $H_2$  control strategies are given as a function of the weighting parameter,  $R$ . In the MPC scheme, the value of prediction horizon,  $p$ , is varied to take the following values: 1, 5, 10, 15 and 20. The control horizon,  $\lambda$ , is kept smaller than the selected prediction horizon. These are chosen accordingly to be 1, 2, 2, 3 and 4. Control forces are kept at a constant level between the end of the predictive and control horizons, i.e.  $u(k + \lambda + i|k) = u(k + \lambda|k)$ ,  $\lambda + 1 \leq i \leq p$ . Figure 13 shows that the control performance depends on the value of the prediction horizon ( $p$ ) or the weighting matrix ( $\mathbf{R}$ ). On one hand, the increase in  $\mathbf{R}$  limits the control force, which results in less displacement reduction. On the other hand, an increase in the prediction horizon results in better control performance. The rms value of the controlled displacement decreases as  $p$  increases although there is a simultaneous increase in the control force. It is

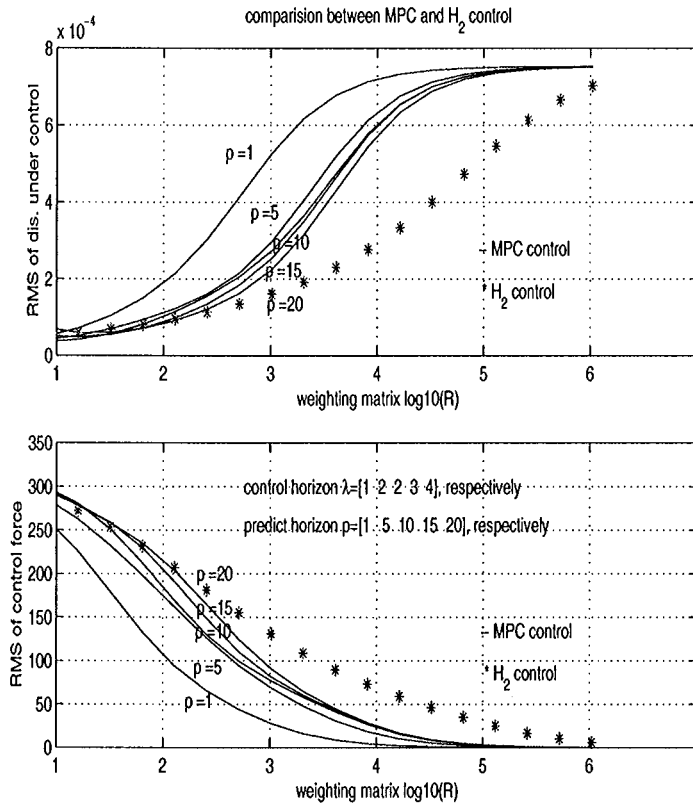


Figure 13. Comparison between MPC and  $H_2$  control (RMS of displacement).

evident that the increased control force decreases the displacement response of the structure. Therefore, better control performance is observed when the prediction horizon is longer.

As the prediction horizon approaches infinity, the cost function of the MPC strategy is close to the  $H_2$  control scheme. Accordingly, the control performance by MPC and  $H_2$  is nearly the same. Figure 13 shows that as the prediction horizon becomes longer, the performance of MPC approaches that of the  $H_2$  control scheme.

Figure 14 shows the control force vs displacement for the  $H_2$  and MPC-AR methods. The results demonstrate that the effectiveness of the  $H_2$  and MPC schemes is equivalent. Using the same control force MPC reduces the displacement response to the level reached by the  $H_2$  control scheme.

The preceding study is repeated with the addition of an on-line AR model as a FF link to the controller design. The results are shown in Figure 15. Figure 15 shows comparison of MPC-AR the scheme and the LQG-AR scheme. The MPC-AR scheme shows a slightly better performance than LQG-AR. The computation efforts used for the MPC-AR scheme is 0.015 s per time step. The computation efforts for the LQG-AR scheme is 0.060 s per time step. For the AR model system identification 0.011 s per time step are needed. So for the MPC-AR scheme, most of the time is consumed in system identification. However, for the LQG-AR model most time is used in solving the Riccati equation.

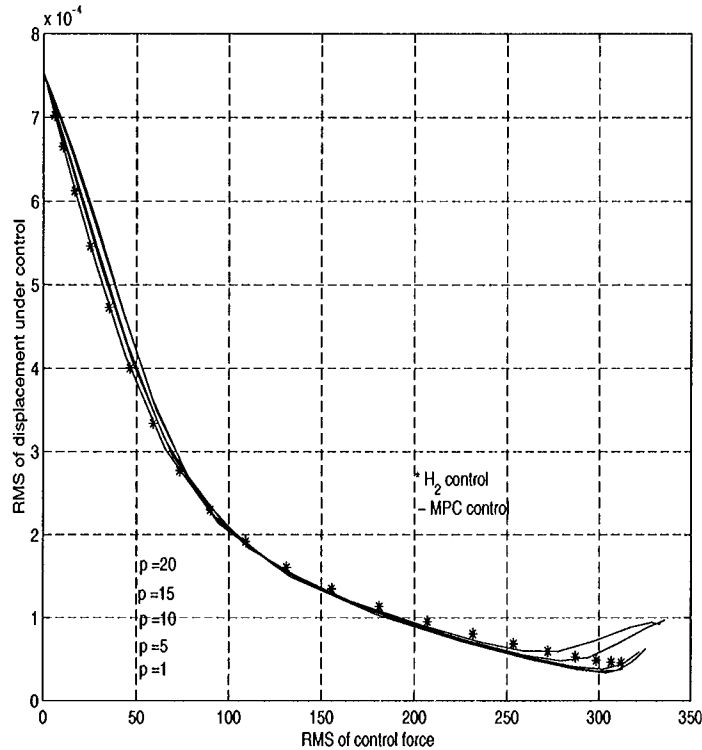


Figure 14. Comparison between MPC and  $H_2$ .

Finally, the Kobe and Hachinohe earthquake acceleration time histories are used as inputs to assess the effectiveness and robustness of the MPC-AR control scheme. As shown in Table III, Figures 16 and 17, the structural response is reduced significantly when the MPC-AR scheme is employed. These results suggest that the MPC-AR model is effective in controlling a wide range of ground accelerations that have their own distinct features.

### 6.3. Analysis of a three-storey building using the MPC-AR model

In this example, a three-storey building [31] is used to demonstrate the MPC-AR scheme using the state FB obtained from each floor of the building. The mass, stiffness and damping matrices of the building are given in Table IV. In this example, the stiffness of the active tendon is  $k_c = 3.7197 \times 10^5$  N/m and  $\alpha = 36^\circ$  (Figure 18). The active tendon is installed at the first floor. In this example,  $Q = I_{(3 \times 3)}$ ,  $p = 5$  and  $\lambda = 2$ .

Like in the previous example, the MPC scheme is first used alone to control the three-storey building which is followed by the MPC-AR scheme. The comparison between the two methods is listed in Table V which shows both the rms and maximum values of the displacement and acceleration of the top floor, and the control force. The weighting matrix is chosen as  $R = 3000$  for the MPC and  $R = 5000$  for the MPC-AR model. Different values of  $R$  are used to ensure that a comparable control force is generated in both cases. Table V shows that

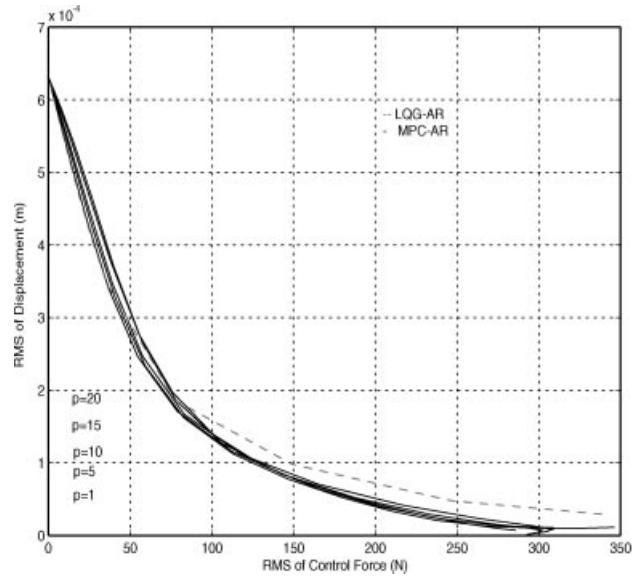


Figure 15. Control performance of LQG-AR and MPC-AR with different prediction and control horizons.

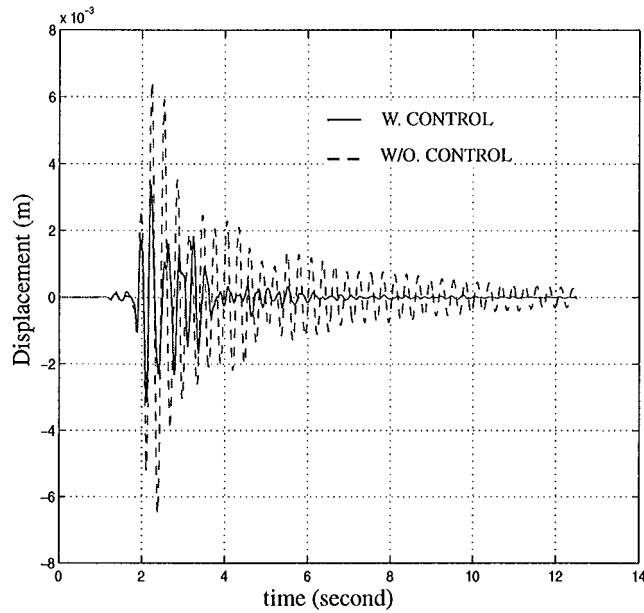


Figure 16. MPC-AR scheme under Kobe earthquake excitation ( $\lambda = 2, p = 5, R = 100$ ).

Table III. Performance of MPC-AR scheme under Kobe and Hachinohe earthquakes.

	$\sigma_x$ (cm)	$\sigma_{\dot{x}}$ (cm/s <sup>2</sup> )	$\sigma_u$ (kN)	$x_{\max}$ (cm)	$\dot{x}_{\max}$ (cm/s <sup>2</sup> )	$u_{\max}$ (kN)
Kobe earthquake	Without control	0.126	68.8	0.67	466.9	
	MPC-AR	0.0541	40.4	0.35	307.5	2.31
	Percentage change	56.9%	41.3%	47.8%	34.1%	
Hachinohe earthquake	Without control	0.0913	45.8	0.21	106.3	
	MPC-AR	0.0277	16.7	0.10	71.19	0.282
	Percentage change	69.6%	63.6%	52.4%	33.0%	

Table IV. Mass, stiffness, and damping matrices of the example building.

Parameters	Values
Mass matrix $M$ (kg)	$M = \begin{bmatrix} 974 & 0 & 0 \\ 0 & 974 & 0 \\ 0 & 0 & 974 \end{bmatrix}$
Stiffness matrix $K$ (N/m)	$K = \begin{bmatrix} 2.7405 & -1.6409 & 0.3690 \\ -1.6409 & 3.0209 & -1.6241 \\ 0.3690 & -1.6241 & 1.3331 \end{bmatrix} \times 10^6$
Damping matrix $C$ (N-s/m)	$C = \begin{bmatrix} 382.65 & -57.27 & 61.64 \\ -57.27 & 456.73 & -2.63 \\ 61.64 & -2.63 & 437.29 \end{bmatrix}$

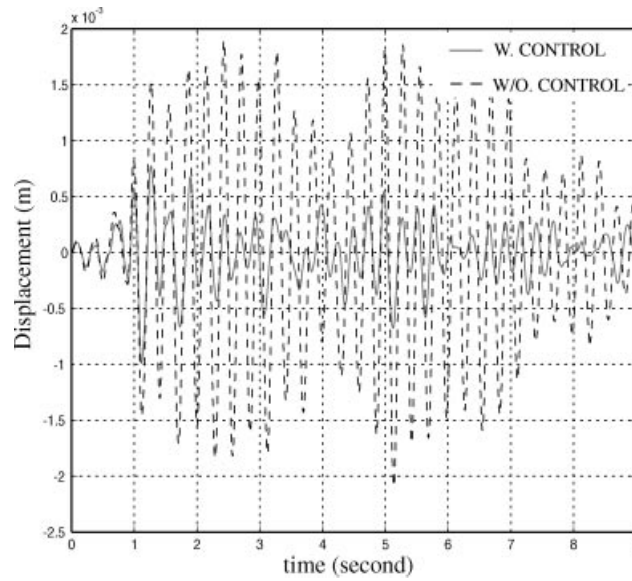


Figure 17. MPC-AR scheme under Hachinohe earthquake excitation ( $\lambda=2, p=5, R=100$ ).

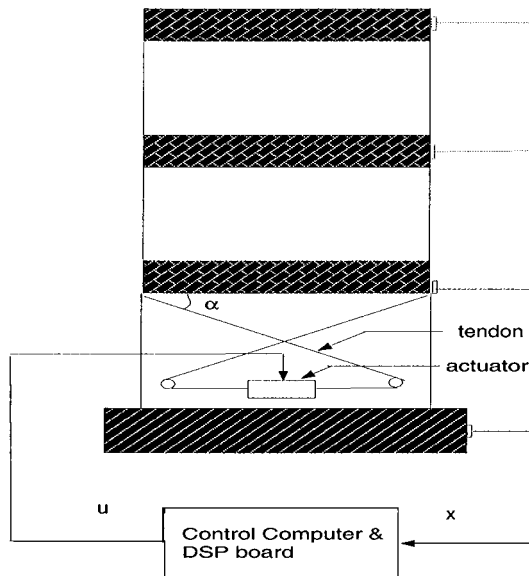
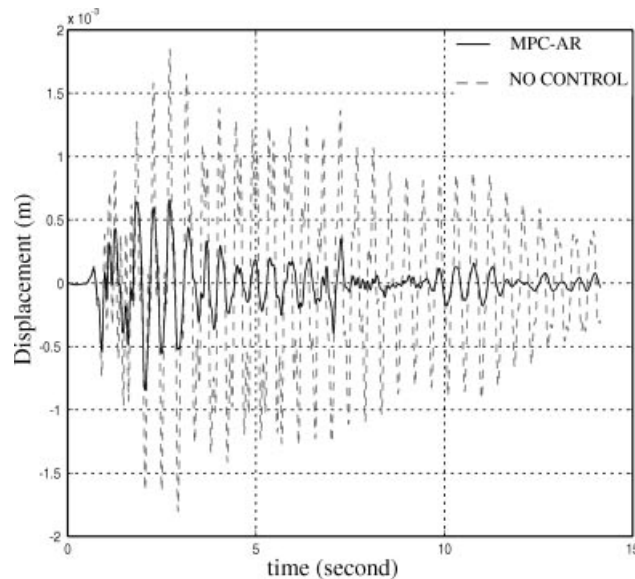


Figure 18. 3-storey building using active tendon control.

with a smaller control force, the MPC-AR scheme offers a better control action than MPC alone. Both the rms and maximum response values obtained using MPC-AR are lower than those obtained using MPC alone. This further points at the superiority of the FF-FB control

Table V. Comparison of MPC-AR and MPC schemes using a three-storey building.

Third floor response	$\sigma_x$ (cm)	$\sigma_{\ddot{x}}$ (cm/s <sup>2</sup> )	$\sigma_f$ (kN)	$x_{\max}$ (cm)	$\ddot{x}_{\max}$ (cm/s <sup>2</sup> )	$f_{\max}$ (kN)
Uncontrolled	0.16	46.5	—	0.38	154.6	—
MPC	0.0602 (62.4%)	22.1 (52.4%)	0.106	0.26 (32.4%)	143.2 (7.4%)	0.517
MPC-AR	0.0518 (67.6%)	17.7 (61.9%)	0.092 (-14.3%)	0.22 (43.0%)	138.4 (10.5%)	0.441 (-14.7%)

Figure 19. Comparison of uncontrolled first floor displacement with MPC-AR scheme ( $\lambda = 2$ ,  $p = 5$ ,  $R = 5000$ ).

using MPC-AR over MPC with FB only. The controlled response of the structure is shown in Figures 19–22. Figures 19 and 20 show the displacement of the first and top floors of the building, respectively, whereas, Figures 21 and 22 show the acceleration of the first and top floors of the building, respectively. The dashed lines represent the uncontrolled case, and the solid lines represent the controlled response using the MPC-AR scheme. Figure 23 shows the control force needed in this example.

This example has demonstrated how the MPC-AR model can effectively control multi-degree-of-freedom systems. On the Sun Sparc Ultra 30 workstation, the three-storey building took 0.002 s for each time step if MPC was used alone and 0.019 s for each time step for MPC-AR model. Because the AR model is estimated at each time step, system identification used up most of the time involved. More efficient AR identification schemes are being considered to further reduce the computational effort for digital implementation of this scheme in scale experiments. The availability of high-speed actuators and computers has made it possible to

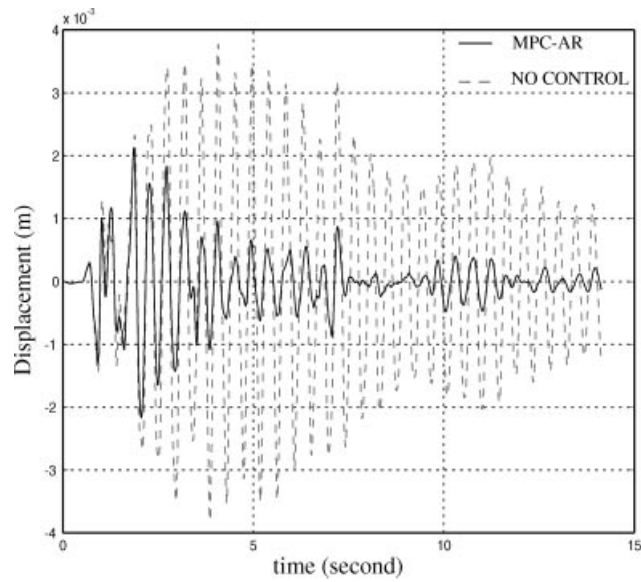


Figure 20. Comparison of uncontrolled top floor displacement with MPC-AR scheme ( $\lambda = 2, p = 5, R = 5000$ ).

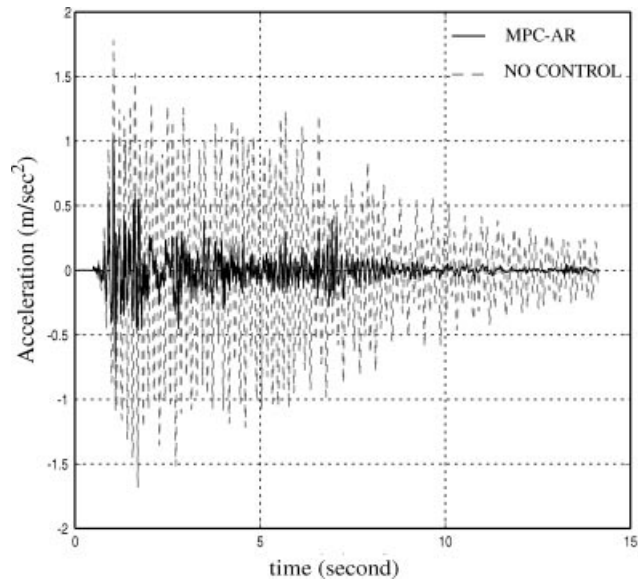


Figure 21. Comparison of uncontrolled first floor acceleration with MPC-AR scheme ( $\lambda = 2, p = 5, R = 5000$ ).

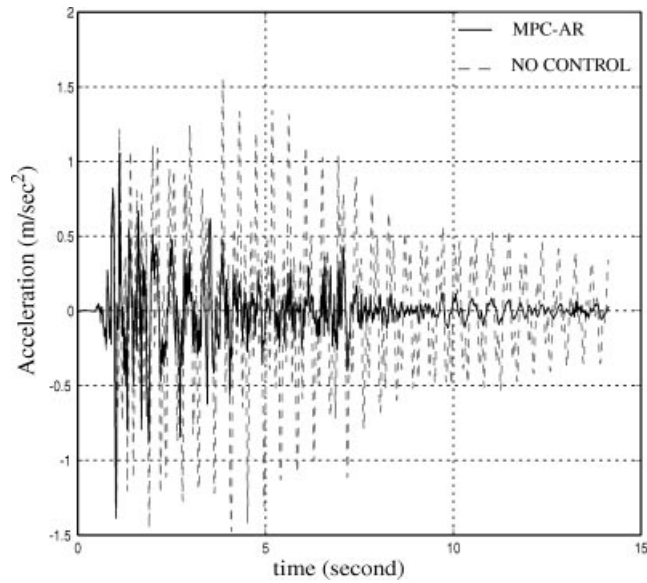


Figure 22. Comparison of uncontrolled top floor acceleration with MPC-AR scheme ( $\lambda = 2$ ,  $p = 5$ ,  $R = 5000$ ).

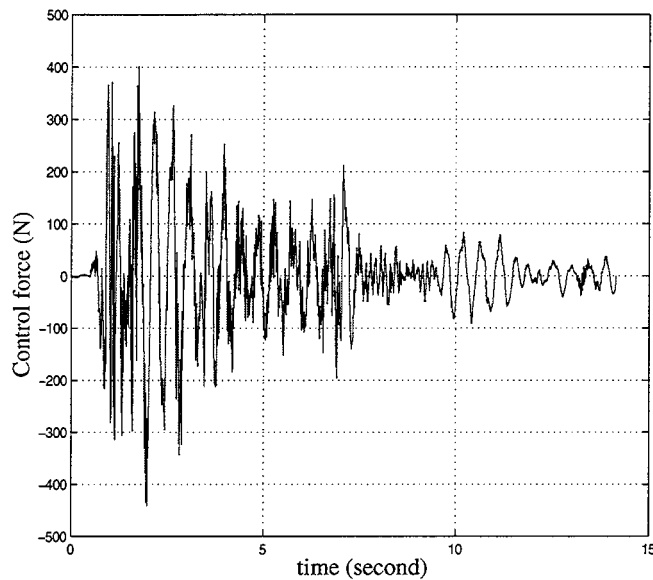


Figure 23. Control force using MPC-AR scheme ( $\lambda = 2$ ,  $p = 5$ ,  $R = 5000$ ).

explore the potentials of MPC scheme which promises to enhance our ability to improve the performance of structure under extreme loads.

### 7. CONCLUSION

In this paper, a real-time model predictive control (MPC) was applied to reduce structural response under earthquake induced loads. First MPC with only a FB scheme was presented. Second, the MPC scheme including both the FB and FF scheme was formulated. Two types of input were used to represent the FF loop in this approach. First, the Kanai–Tajimi model was used, which represented the FF loop based on the established earthquake spectral characteristics. Second, the MPC-AR scheme was introduced in which actual real-time measurements obtained on-line were utilized to model the FF component. The FF model using these two methodologies were then augmented with the equations of motion of the structure to determine the FF–FB gains.

This study clearly demonstrated the effectiveness of the general MPC strategy for reducing structural response and associated load effects under earthquake loads. The performance of MPC in the infinite horizon case was shown to be comparable to the  $H_2$  strategies. In addition, the MPC scheme is easier to implement in a digital control application that utilizes real-time measurements of excitation. A parameter study was also conducted to delineate the influence of different weighting factors on the control force, and prediction and control horizons.

MPC with the FF–FB components clearly enhanced the performance of the controller, e.g. the Kanai–Tajimi model provided an improved reduction in the response when compared to MPC with FB only. However, since this method depends on a prescribed spectral model of earthquake, it may not always yield satisfactory performance for earthquakes with features that differ from those captured in this model. This shortcoming can be alleviated by an MPC-AR-based FF–FB scheme, which can be employed in real time for any earthquake input. The results obtained using the MPC-AR scheme showed further improvement over MPC with only FB.

This paper has demonstrated the efficacy of MPC scheme in controlling structural motions under earthquakes and provided the framework for capturing the attractive features of MPC, i.e. computational expediency and real-time applications. An attractive feature of MPC concerning its intrinsic ability to include constraints in the design process is being currently examined by the authors for structural control applications.

### APPENDIX

$$H = \begin{bmatrix} H_1 & 0 & \dots & 0 \\ \dots & \dots & \dots & \dots \\ H_\lambda & H_{\lambda-1} & \dots & H_1 \\ H_{\lambda+1} & H_\lambda & \dots & H_1 + H_2 \\ \dots & \dots & \dots & \dots \\ H_p & H_{p-1} & \dots & H_1 + \dots + H_{p-\lambda} \end{bmatrix}, \quad H_k = C\hat{\Phi}^{k-1}\hat{\Gamma}_u \quad (A1)$$

$$Y_z = [(C\hat{\Phi})^T (C\hat{\Phi}^2)^T \dots (C\hat{\Phi}^p)^T]^T \quad (\text{A2})$$

$$Y_e = \left[ (C\hat{\Gamma}_e)^T (C(I + \hat{\Phi})\hat{\Gamma}_e)^T \dots \left( C \sum_{k=1}^p (\hat{\Phi}^{k-1})\hat{\Gamma}_e \right)^T \right]^T \quad (\text{A3})$$

$$Y_d = \left[ H_{v1}^T H_{v1}^T + H_{v2}^T \dots \sum_{k=1}^p H_{vk}^T \right]^T, \quad H_{vk} = C\hat{\Phi}^{k-1}\hat{\Gamma}_d \quad (\text{A4})$$

and

$$\bar{Q} = \begin{bmatrix} Q & \dots & 0 \\ \dots & \dots & \dots \\ 0 & \dots & Q \end{bmatrix}, \quad \bar{R} = \begin{bmatrix} R & \dots & 0 \\ \dots & \dots & \dots \\ 0 & \dots & R \end{bmatrix}, \quad Q = \begin{bmatrix} I & 0 \\ 0 & 0 \end{bmatrix}, \quad R = I \quad (\text{A5})$$

#### ACKNOWLEDGEMENTS

The support for this work was provided in part by the National Science Foundation Grants CMS-94-02196 and CMS-95-03779 under the NSF Structure Control Initiative. This support is gratefully acknowledged.

#### REFERENCES

1. Soong TT. *Active Structural Control: Theory and Practice*. Longman Scientific and Technical: Essex, England, 1990.
2. Suhardjo J, Spencer Jr BF, Kareem A. Frequency domain optimal control of wind excited buildings. *ASCE, Journal of Engineering Mechanics* 1992; **118**(12):2463–2481.
3. Yang JN, Wu JC, Reinhorn AM, Riley M, Schmitendorf WE, Jabbari F. Experimental verifications of  $H_\infty$  and sliding mode control for seismic-excited buildings. *Proceedings of First World Conference on Structure Control*, TP4, 1994; 63–72.
4. Spencer Jr BF, Dyke SJ, Doeskar HS. Benchmark problem in structural control Part 1: active mass driver system, and Part 2: active tendon system. *Earthquake Engineering and Structural Dynamics* 1998; **27**(11):1127–1147.
5. Suhardjo J, Kareem A. Structural control of offshore platforms. *Proceedings of the 7th International Offshore and Polar Engineering Conference ISOPE-97*, Honolulu May 25–30, 1997.
6. Kijewski T, Kareem A, Tamura Y. Overview of methods to mitigate the response of wind-sensitive structures. *Proceedings of Structural Engineering World Congress*. San Francisco, July 19–23, 1998.
7. Soong TT. Structural control: impact on structural research in general. *Proceedings of Second World Conference on Structural Control*, vol. 1, 1998; 5–14.
8. Structural Control. *Proceedings of First World Conference on structural Control*, vols. 1–3, 1994.
9. Structural Control. *Proceedings of Second World Conference on Structural Control*, vols. 1–3, 1998.
10. Housner G, Bergman LA, Caughey TK, Chassiakos AG, Claus RO, Masri SF, Skelton RE, Soong TT, Spencer BF, Yao JTP. Structural control: past, present, and future. *ASCE, Journal of Engineering Mechanics* 1997; **123**(9):897–971.
11. Kareem A, Kijewski T, Tamura Y. Mitigation of motions of tall buildings with specific examples of recent applications. *Wind & Structures* 1999; **2**(3):201–251.
12. Doyle JC, Glover K, Khargonekar P, Francis B. State-space solutions to standard  $H_2$  and  $H_\infty$  control problems. *IEEE Transactions on Automatic Control* 1989; **34**:831–847.
13. Suhardjo J, Spencer Jr BF, Sain MK. Feedback–feedforward control of structures under seismic excitation. *Structural Safety* 1990; **8**:69–89.
14. Dyke JS. Acceleration feedback control strategies for active and semi-active control systems: modeling, algorithm development and experiment verification. *Ph.D. Dissertation*, University of Notre Dame.

15. Wu, JC, Yang JN, Schmitendorf W. Reduced order  $H_\infty$  and LQR control for wind excited tall buildings. *Engineering Structures* 1998; **20**(3):222–236.
16. Utkin VI. Variable structure systems with sliding modes. *IEEE Transactions on Automatic Control* 1977; **AC-22**:212–222.
17. Slotine JJE. Sliding controller design for nonlinear systems. *International Journal of Control* 1984; **40**:No. 2.
18. Rodellar J, Barbat AH, Matin-Sanchez JM. Predictive control of structures. *ASCE, Journal of Engineering Mechanics* 1987; **113**(6):797–812.
19. Lopez-Almansa F, Andrade R, Rodellar J, Reinhorn AM. Modal predictive control of structures I: formulation. *ASCE, Journal of Engineering Mechanics* 1994; **120**(8):1743–1760.
20. Lopez-Almansa F, Andrade R, Rodellar J, Reinhorn AM. Modal predictive control of structures II: implementation. *ASCE, Journal of Engineering Mechanics* 1994; **120**(8):1761–1772.
21. Yamada K, Kobori T. Linear quadratic regulator for structure under on-line predicted future seismic excitation. *Earthquake Engineering and Structural dynamics* 1996; **25**:631–644.
22. Mei G, Kareem A, Kantor JC. Real-time model predictive control of structures under earthquakes. *Proceedings of Second World Conference on Structural Control*, vol. 2, 1998; 1585–1594.
23. Yoshida K, Yoshida S, Takeda Y. Semi-active control of base isolation using feedforward information of disturbance. *Proceedings of Second World Conference on Structure Control*, vol. 1, 1998; 377–386.
24. Ricker L. Model predictive control with state estimation. *Industrial and Engineering Chemistry Research* 1990; **29**:374–382.
25. Morari M, Garcia CE, Lee DM, Prett DM. *Model Predictive Control*. Prentice-Hall: Englewood Cliffs, NJ, 1994.
26. Qin SJ, Badgwell TJ. An overview of industrial model predictive control technology. In *Chemical Process Control—V.*, Proceedings published as *AIChE Symposium Series* 316, vol. 93. CACHE and AIChE, 1996; 232–256.
27. Camacho EF, Bordons C. *Model Predictive Control*. Springer: London, 1999.
28. Clough RW, Penzien J. *Dynamics of Structures* (2nd edn). McGraw-Hill, Inc: New York, 1993.
29. Deodatis G, Shinozuka M. Auto-regressive model for nonstationary stochastic processes. *ASCE, Journal of Engineering Mechanics* 1988; **114**(11):1995–2012.
30. Dyke JS, Spencer Jr BF, Quast P, Sain MK. The role of control-structure interaction in protective system design. *Journal of Engineering Mechanics, ASCE* 1995; **121**(2):322–338.
31. Chung LL, Lin RC, Soong TT, Reinhorn AM. Experimental study of active control for MDOF seismic structures. *ASCE, Journal of Engineering Mechanics* 1989; **115**(8):1609–1627.